URSI GASS 2023, Sapporo, Japan, 19 – 26 August 2023

CLIMF2: A Climatological Model of the Ionospheric F2 Layer

Danielle J. Edwards* (1), Thomas E. Chambers(2), and Manuel A. Cervera(1,2)
(1) Defence Science and Technology Group, Edinburgh, Australia; e-mail: danielle.edwards@defence.gov.au; manuel.cervera@defence.gov.au
(2) The University of Adelaide, Adelaide, Australia; e-mail: thomas.chambers@adelaide.edu.au

Abstract

The ionospheric F2 layer is of key importance to systems dependent on the propagation of radio waves through the ionosphere. The currently accepted climatological F2 layer model, the International Reference Ionosphere (IRI), has a limitation: it does not model the variance in the F2 layer. Our newly developed model, CLIMF2, is intended to overcome this limitation, and thus improve applications such as the climatological modelling of over-the-horizon (OTH) radar performance. CLIMF2 is an empirical climatological monthly median model of the F2 layer derived from a global network of vertical incidence sounders (VIS) observations, consisting of 267 sites with data from the 1950s to 2021. The models of foF2 and hmF2 in CLIMF2 and IRI perform relatively similarly, but CLIMF2 shows improvements over IRI, especially around sunrise. CLIMF2 has the added functionality of providing the variance in the foF2 and hmF2 parameters. CLIMF2 also models the F2 layer B0 and B1 parameters, which will be discussed in a further paper.

1 Introduction

The F2 layer of the Earth's ionosphere exhibits dynamic variability on time scales ranging from minutes to years, and spatial scales of meters to thousands of kilometers [1]. Contributing to this variability are a wide range of physical processes of both terrestrial and solar origin. Hence, empirical models are essential in characterizing this atmospheric layer. The development and evaluation of such a model is presented within this paper.

The International Reference Ionosphere (IRI) is currently the most widely accepted and used empirical climatological model of the ionosphere [2, 3]. However, the incorporated model of the F2 layer has limitations relating to the scope of input observations and is unable to model the variance of the ionospheric layer parameters [2]. Knowledge of this variability is critical for the climatological modelling of the performance of HF systems.

The Climatological Model of the F2 region (CLIMF2), developed and presented in this paper, is intended to be used in conjunction with IRI. One of the functional modes of IRI allows for user input of the critical frequency (foF2) and/or the height of the peak electron density (hmF2) of the ionospheric F2 layer. This allows for the generation of ionospheric profiles by IRI, but with the CLIMF2 parameters of the F2 layer at either the monthly median, upper decile or lower decile levels.

2 Data

CLIMF2 is developed from a global network of vertical incidence sounder (VIS) observations from: the World Data Center (WDC) [4], the Global Ionospheric Radio Observatory (GIRO) [5], and the Jindalee Operational Radar Network (JORN) VIS sounders [6]. This combined sounder network, shown in Figure 1, currently includes 267 sites with data ranging from the 1950s to 2021. Despite reasonably good global coverage of observations, there are still regions that are under-sampled, such as certain longitude sectors of the equatorial region, the auroral regions, and the oceans.

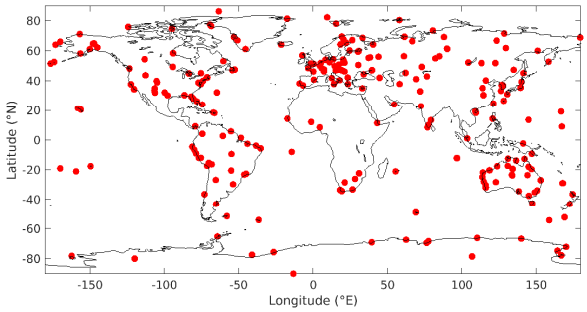

Figure 1**.** Locations of the 267 VIS sites contributing to the CLIMF2 input dataset.

3 Method

CLIMF2 is an empirical climatological model driven by a global network of VIS observations first reported on by [7] and then by [8]. The VIS data are filtered using quality control flags [7], and times of geomagnetic storms are removed using the disturbance storm time (DST) index [7, 9]. The VIS data are then binned by UTC hour, month and the S12 solar sunspot number [10]. Five solar bins of varying widths are used: S12 0-20, 20-40, 40-80, 80-150, and >150. The variable widths of these bins account for the reduction in observations in the higher solar regime bins due to solar storm filtering rejection. The model also allows for the use of other solar parameters such as the F10.7 radio flux but this is not discussed further here.

The monthly median and upper and lower deciles are calculated for the F2 layer parameters for each bin. In this paper we will focus on the foF2 and hmF2, but note that the B0 and B1 parameters are also modelled. Linear interpolation is used to interpolate these statistics to the centers of the solar bins.

The data from all sites and bins are then further processed to shift from UTC to local solar time (LST) using the solar zenith angle at each site. Local solar noon is defined as the time when the solar zenith angle is at a minimum for the day. This treatment of the data collapses the longitude dimension and allows us to fit a simple 1D function to the data against an appropriate parameter that captures the latitudinal variation. As the geomagnetic field influences plasma transport in the F2 region, we chose modified dip angle (modip) as that parameter [11].

Chebyshev polynomials of the first kind were chosen for the modip fit, following the work of [8]. A sequence of fits with order increasing up to a maximum fit order of 21 were performed for each statistic of the F2 parameters at each hour, month and solar regime bin. The optimal fit was then chosen using the degrees of freedom adjusted R-squared statistic. The fit order with the maximum value for the degrees of freedom adjusted R-squared value was chosen and the fit coefficients were saved.

To improve the performance of these fits in data sparse regions, data from the northern hemisphere from latitudes greater than 60 degrees were copied to the southern hemisphere adjusting appropriately for modip and season. The data was also mirrored across the poles to ±120 degrees (adjusting for time of day) and linear interpolation was used between the points nearest the pole. This was done to control the Chebyshev fit at the extremities and thus improve the performance of the fits at the poles. An example of this fitting is shown in Figure 2.

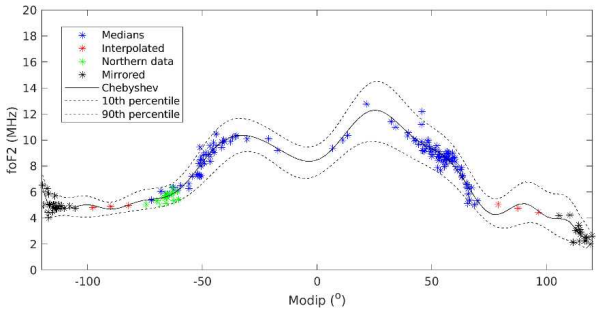

Figure 2. Example of a fit of foF2 as a function of Modip. The dashed lines show the optimal fits to the 10th and 90th percentile data. Fit for S12 = 115, in January at 11 UT.

4 Results

An important capability of CLIMF2 is the ability to model the variance in the foF2 and hmF2. The upper and lower deciles of these parameters can be calculated along with the monthly median, as shown for foF2 in Figure 3. The minimisation of unphysical overfitting biases and qualitative tests such as the ability of the model to realistically capture general phenomena, for example the Equatorial Ionospheric Anomaly (EIA), were used to verify the model is performing as expected.

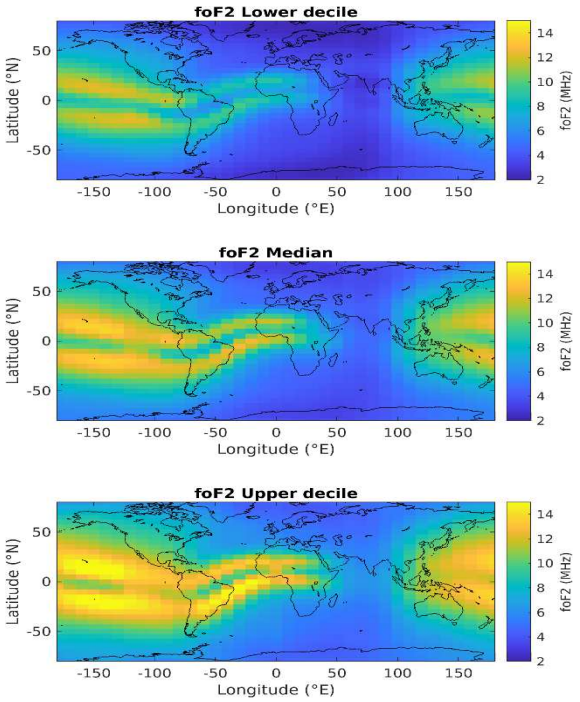

Figure 3. Global plots of the foF2 lower deciles (top), medians (middle) and upper deciles (bottom) from CLIMF2. This example is for S12 = 94 in March at 0 UT.

A comparison of the CLIMF2 and IRI foF2 models in January at sunspot number 94 is shown in Figure 4. Both models present similar large-scale features which shows the expected diurnal behavior, although there are notable differences, such as seen around 10°N, -150°E. The two models were compared over the year and solar cycle, with similar large-scale behaviors observed throughout for both the foF2 and hmF2.

An analysis of the performance of CLIMF2 against the foF2 and hmF2 measurements from ionospheric sounders is required to validate the CLIMF2 model. The foF2 and hmF2 modelled using both CLIMF2 and IRI were compared against the filtered and binned data from each of the VIS sites. The median foF2 and hmF2 were modelled hourly for each month of the year for S12 values of 10, 30, 60, 115, and 200. IRI's SDMF2 [12] model of hmF2 was used to generate the IRI hmF2 data. Note that IRI uses the R12 sunspot number, where R12 ≈ 0.7*S12 [13]. CLIMF2 was regenerated with sets of 10 random VIS sites removed for comparison against those VIS sites, so the data used for validation was not contributing to the model. The residuals and cross correlation lags between the models and the VIS observations were calculated as described by [7]. The mean and the standard deviation of the residuals, and the mean of the cross-correlation lags across all the epochs (i.e. 12 months x 5 SSN bins) were calculated for each site to investigate global biases in the models.

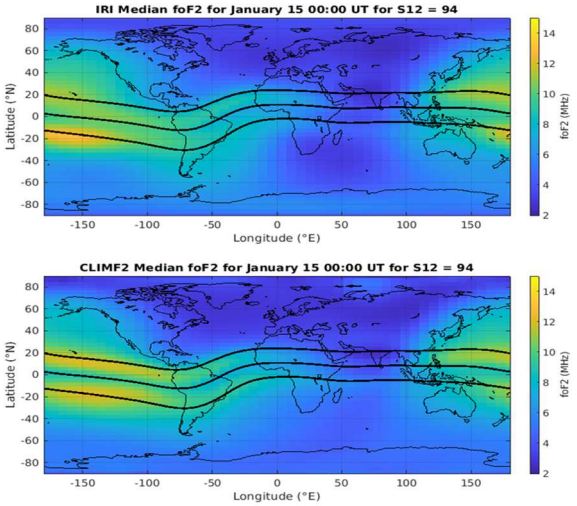

Figure 4. Comparison between the IRI CCIR model (top) and CLIMF2 (bottom) median foF2. The models are evaluated at SSN = 94 for January 00:00Z. The solid black lines indicate the magnetic equator (central line) and magnetic dip angles of ±15°.

Maps of the foF2 residuals and lags are shown in Figure 5 with histograms of those values in Figure 6. We note that CLIMF2 and IRI perform similarly with a slight improvement for the CLIMF2 foF2 model as evidenced by a small shift to lower values in the CLIMF2 histograms (orange) in comparison to the IRI histograms (blue). Figure 7 and 8 display the same plots for hmF2. From these histograms, we see a more definite trend of the CLIMF2 histograms to lower values and so we conclude that the CLIMF2 hmF2 model performs better than IRI. The same analysis was also performed using IRI's AMTB hmF2 model, which showed an obvious positive bias in the hmF2 globally, as has been shown by [2] and others.

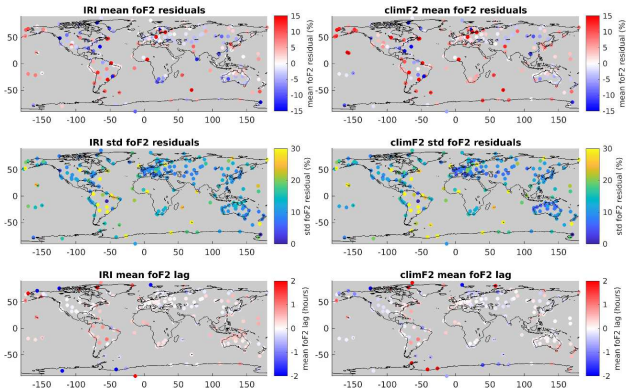

Figure 5. Map of the mean (top) and standard deviation (middle) of the residuals and the mean cross correlation lag (bottom) between the IRI CCIR (left) and CLIMF2 (right) modelled foF2 and the observations from all VIS sites.

The residuals and lags were also investigated for various seasons and sunspot numbers, with the results for each epoch similar to the entire dataset analysis described above. Both the CLIMF2 and IRI models of the foF2 performed better in summer than in winter, while the performance showed little dependence on the sunspot number. Conversely, the performance of the hmF2 models of both CLIMF2 and IRI showed little dependence on the season, with slightly better performance seen at lower sunspot numbers.

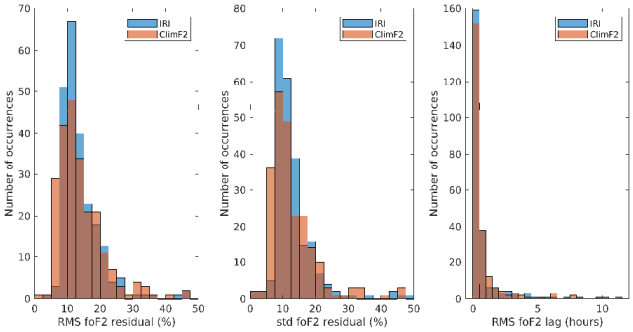

Figure 6. Histograms of the mean (left) and standard deviation (middle) of the residuals and the mean cross correlation lag (right) between the IRI CCIR (blue) and CLIMF2 (orange) modelled foF2 and the observations from all VIS sites.

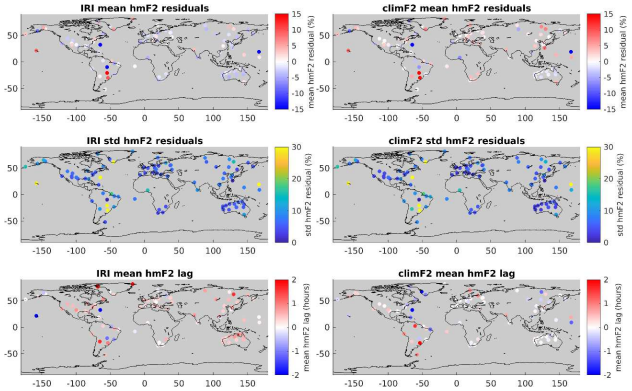

Figure 7. Map of the mean (top) and standard deviation (middle) of the residuals and the mean cross correlation lag (bottom) between the IRI SDMF2 model (left) and CLIMF2 (right) modelled hmF2 and the observations from all VIS sites.

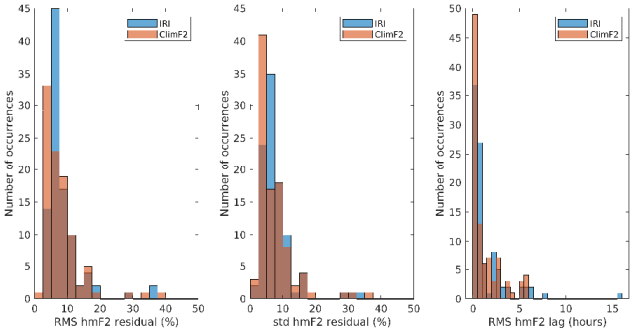

Figure 8. Histograms of the mean (left) and standard deviation (middle) of the residuals and the mean cross correlation lag (right) between the IRI SDMF2 model (blue) and CLIMF2 (orange) modelled hmF2 and the observations from all VIS sites.

The performance of the models with the time of day was investigated using a 2D histogram of the residuals for all locations, sunspots and months versus the hour of day, as shown in Figure 9. Both CLIMF2 and IRI generally have a greater range of residuals between the modelled and observed foF2 at night than during the day (Figure 9 top panels). IRI tends to underestimate the foF2 more as the night goes on (seen in the decreasing residuals between 0 and 5 LST), and then overestimate the foF2 (at around 7 LST) before more closely agreeing with the observed foF2. This behavior of IRI has been previously reported for locations in China [14] and is not observed in CLIMF2.

CLIMF2 does not show any strong hourly variation in the hmF2 residuals (Figure 9 bottom left panel). However, the hmF2 residuals from IRI (Figure 9 bottom right panel) become more negative at night, with IRI underestimating the hmF2 before sunrise and then quickly recovering to match the VIS observations closer.

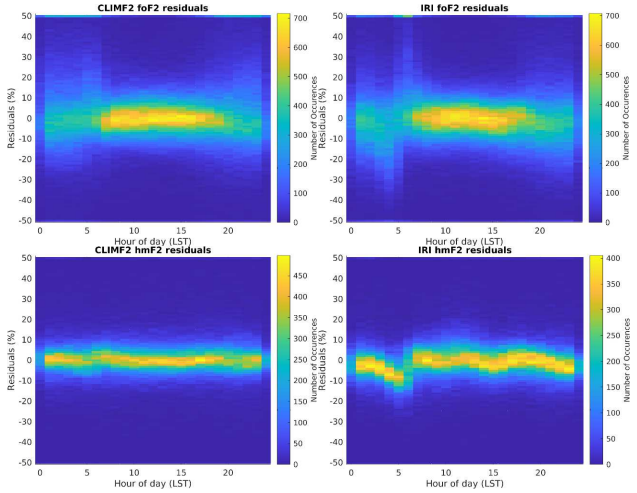

Figure 9. 2D histograms of the CLIMF2 (left) and IRI (right) foF2 (top) and hmF2 (bottom) residuals versus the time of day for all VIS sites. The 50% residual bin includes values >50.

5 Conclusions

The development and evaluation of a climatological model of the ionospheric F2 layer is presented within this paper. This model provides the ability to obtain the variance in the F2 layer parameters. This is essential for complete HF radar climatological performance modelling and is not currently available in IRI. Improvements in the modelled foF2 and hmF2 were found in comparison with IRI, especially around sunrise.

Acknowledgements

We are grateful to the Australian Bureau of Meteorology, Space Weather Services for the provision of scaled hourly ionospheric data. We acknowledge using data of the Lowell Global Ionospheric Radio Observatory Data Centre (http://spase.info/SMWG/Observatory/GIRO). All available ionospheric data was used, as acknowledged at https://giro.uml.edu/didbase/acknowledgements.htm.

References

[1] R. Gardiner-Garden *et al.*, "A description of the Elevation sensitive Oblique Incidence Sounder Experiment (ELOISE)," *Advances in Space Research,* vol. 64, no. 10, pp. 1887-1914, 2019, doi: 10.1016/j.asr.2019.03.036.

[2] D. Bilitza, M. Pezzopane, V. Truhlik, D. Altadill, B. W. Reinisch, and A. Pignalberi, "The International Reference Ionosphere Model: A Review and Description of an Ionospheric Benchmark," *Reviews of Geophysics,* vol. 60, no. 4, p. e2022RG000792, 2022, doi: https://doi.org/10.1029/2022RG000792.

[3] D. Bilitza, "IRI the International Standard for the Ionosphere," *Advances in radio science,* vol. 16, pp. 1-11, 2018, doi: 10.5194/ars-16-1-2018.

[4] *Ionospheric Data- Hourly*. [Online]. Available: https://www.sws.bom.gov.au/World_Data_Centre/1/3

[5] B. W. Reinisch and I. A. Galkin, "Global Ionospheric Radio Observatory (GIRO)," *Earth, planets and space,* vol. 63, no. 4, pp. 377-381, 2011, doi: 10.5047/eps.2011.03.001.

[6] A. Cameron, "The Jindalee operational radar network: its architecture and surveillance capability," presented at the Proceedings International Radar Conference, Alexandria, VA, USA, 1995.

[7] D. Field, "A new empirical climatological model of ionospheric foF2 and hmF2 and review of the International Reference Ionosphere," School of Physical Sciences, The University of Adelaide, 2018.

[8] T. Chambers and M. Cervera, "Development of a Climatological Model of the Ionospheric F2 Layer," Defence Science and Technology Group, Australia, DSTG-TR-3927, 2022.

[9] M. Nose, T. Iyemori, M. Sugiura, and T. Kamei. *Geomagnetic Dst index*, doi: 10.17593/14515-74000.

[10] SILSO World Data Center, "The International Sunspot Number," *International Sunpot Number Monthly Bulletin and online catalogue,* 1950-2021. [Online]. Available: http://www.sidc.be/silso/.

[11] D. Bilitza, "International reference ionosphere 1990," National Space Science Data Centre, Legacy CDMS, 1990, vol. 90-22.

[12] V. N. Shubin, "Global median model of the F2-layer peak height based on ionospheric radio-occultation and ground-based Digisonde observations," *Advances in space research,* vol. 56, no. 5, pp. 916-928, 2015, doi: 10.1016/j.asr.2015.05.029.

[13] F. Clette and L. Lefèvre, "The New Sunspot Number: Assembling All Corrections," *Solar physics,* vol. 291, no. 9-10, pp. 2629-2651, 2016, doi: 10.1007/s11207-016-1014-y.

[14] Z. Liu, H. Fang, L. Weng, S. Wang, J. Niu, and X. Meng, "A comparison of ionosonde measured foF2 and IRI-2016 predictions over China," *Advances in Space Research,* vol. 63, no. 6, pp. 1926-1936, 2019/03/15/ 2019, doi: https://doi.org/10.1016/j.asr.2019.01.017